Theoretical Dimension and the Complexity of Simulated Turbulence

Mladen Victor Wickerhauser[1], Marie Farge[2], and Eric Goirand[3]

Abstract. A global quantity called "theoretical dimension" is roughly proportional to the number of coherent structures that expert observers count in simulated two-dimensional turbulent viscous flows. This paper reviews some previously published computations of this quantity for a few academic examples and for a small number of flows computed from random initial vorticity fields.

§1 Introduction

Evolution equations describing complicated phenomena like turbulence and nonlinear wave propagation sometimes produce coherent features such as shock fronts and traveling vortices. These coherencies permit an approximate description of the evolving state by relatively few parameters, regardless of how many free parameters were initially used in the numerical resolution of the equation. The goal of this paper is to discuss automatic methods for extracting such *low-rank* approximations to complicated phenomena, and to present results of one such method applied to two simple examples: Burgers' equation with dissipation, as previously computed in one spatial dimension [8], and the incompressible Navier–Stokes equation, previously analyzed in two spatial dimensions [7]. New data is contained in Figures 4 and 5, and Tables 2 and 3.

The rank reduction method will be a kind of *lossy compression*; the solution at any instant in time will be written as a superposition of orthogonal *phase atoms*, defined below, and then only those component atoms whose amplitudes exceed some threshold will be retained. *Coherence* will be detected by counting the number of retained components; when this count is low, the instantaneous state will be considered coherent.

To count the relative importance of the retained components in such *phase atom expansions*, their amplitudes will be weighted using the *entropy functional* defined as follows. For any nonzero sequence $a = \{a(n) : n = 0, 1, 2, \ldots\}$ with $\|a\|^2 = \sum_n |a(n)|^2 < \infty$, put

$$H(a) \stackrel{\text{def}}{=} -\sum_n \frac{|a(n)|^2}{\|a\|^2} \log\left(\frac{|a(n)|^2}{\|a\|^2}\right). \tag{1.1}$$

As usual, $0 \log 0$ is evaluated by continuous extension as 0. This is called the "entropy functional" because it is the entropy of the discrete probability distribution given by $p(n) = |a(n)|^2/\|a\|^2$. In [19], p.278, and many other places it is shown that if $M > 0$ is the count of nonzero elements $a(n)$, then $0 \le H(a) \le \log M$, and the maximum value is achieved when all nonzero $a(n)$ have the same magnitude. Thus $H(a)$ measures the *flatness* of the component amplitudes; it will be low when the amplitudes are not flat, *i.e.*, when they are concentrated into fewer than M large components.

Now define the *theoretical dimension* $TD(a)$ of the sequence a by

$$TD(a) \stackrel{\text{def}}{=} \exp H(a). \tag{1.2}$$

put here title
put here (eds.), pp. 1–??.

put here ISBN

This quantity is used to boost intuition about the sequence a, since it can be said to measure the *number of significant amplitudes* rather than their logarithm, which measures the number of bits required to encode them.

Both $H(a)$ and $TD(a)$ are computable for both finite and infinite sequences, so long as the sequences have slightly faster decrease as $n \to \infty$ than required for square-summability. In the experiments below, all sequences a are finitely supported with at most some large number M of nonzero coefficients; in that case, coherence will mean simply that $TD(a) \ll M$.

Phase atoms are smooth functions which are well localized in both position and momentum in the sense of quantum mechanics. Namely, a phase atom $\psi = \psi(x)$ must have the following properties:

- Finite energy:
$$\|\psi\|^2 \stackrel{\text{def}}{=} \int |\psi(x)|^2 \, dx < \infty. \tag{1.3}$$
Without loss, it can be assumed that $\|\psi\| = 1$.

- Smoothness and decay: both ψ and $\hat{\psi}$ are smooth, where $\hat{\psi}$ is the Fourier integral transform of ψ;

- Position and momentum:
$$x_0 \stackrel{\text{def}}{=} \int x|\psi(x)|^2 \, dx < \infty; \qquad \xi_0 \stackrel{\text{def}}{=} \int \xi|\hat{\psi}(\xi)|^2 \, d\xi < \infty; \tag{1.4}$$
these are respectively called the *position* and *momentum* of ψ;

- Localization in position and momentum:
$$\Delta x \stackrel{\text{def}}{=} \left(\int (x - x_0)^2 |\psi(x)|^2 \, dx \right)^{1/2} < \infty; \qquad \Delta\xi \stackrel{\text{def}}{=} \left(\int (\xi - \xi_0)^2 |\hat{\psi}(\xi)|^2 \, d\xi \right)^{1/2} < \infty; \tag{1.5}$$
these are respectively called the *position uncertainty* and *momentum uncertainty* of ψ;

- Concentration: ψ must be approximately as well localized in position and momentum as the Heisenberg uncertainty principle allows, that is,
$$\Delta x \; \Delta\xi \approx 1. \tag{1.6}$$

The *theoretical dimension of a function* f is the minimum value of $TD(a)$ achievable for any sequence a for which
$$f(x) = \sum_n a(n)\psi_n(x) \tag{1.7}$$
and $\{\psi_n\}$ is a collection of phase atoms. Call that quantity $TD(f)$. It is obviously difficult to compute, since there is no simple parameterization of phase atoms over which to optimize, so it must be estimated using some particular, easily computed subset of the phase atom decompositions.

The *matching pursuit* algorithm [12] is one effective way to search over a large library of phase atom decompositions, the Gabor bases. *Adapted waveform analysis* [10, 18] is a fast approximation of matching pursuit which uses *wavelet packets* [4] rather than modulated Gaussians as phase atoms. Both are examples of *meta-algorithms* [16] which fit a decomposition with good analytical properties to a function.

The *best-basis* expansion [5] of a function is a further simplification and speed-up of adapted waveform analysis; it is the phase atom decomposition used here to obtain an approximation for $TD(f)$.

To estimate the evolving complexity of a numerical simulation using the notion of theoretical dimension, suppose that $f = f(x, t_0)$ is the solution at a fixed time t_0. Then $TD(f)$ is estimated using a reasonable library of phase atoms and the result plotted as a function of t_0. Progress through states of instantaneous coherence will be seen as local minima, and incoherence will be seen as local increases of TD.

The remainder of this paper is divided into three parts. In the first, the techniques used to compute solutions to two evolution equations are described, as well as the algorithm for approximating $TD(f)$ for each instant in time using wavelet packet best-basis expansions. In the second, numerical results from two simultations are presented. In the third, there is a brief discussion of the interpretation of the results and comments on how the technique might be improved.

§2 Techniques

2.1 Wavelet packet best basis expansions

Wavelet packets are generalizations of the compactly-supported *wavelets* introduced by Daubechies, Mallat, and Meyer [6, 11, 15]. They constitute an over-abundant set of basis functions with remarkable orthogonality properties, namely, that very many subsets form orthonormal bases. The one-dimensional functions were first described in Reference [4]. Each basis element ψ is characterized by three attributes: scale s, wavenumber k, and position p, so they may be labeled ψ_{skp}. By the Heisenberg uncertainty principle, it is not possible to localize a function to arbitrary precision in both p and k. In other words, $\Delta p \cdot \Delta k \geq 1$ in normalized units, where Δp is the uncertainty in position and Δk is the uncertainty in momentum. In the wavelet packet construction, $\Delta p \approx 2^s$ and $\Delta k \approx 2^{-s}$ in the same normalization, so that the product of the uncertainties is roughly as small as possible. Such functions, which cannot be significantly better localized in phase space, are evidently phase atoms.

Fourier analysis with such waveforms or atoms consists of calculating the *wavelet packet transform* $w_{skp}(f) = \langle \psi_{skp}, f \rangle$. Certain subsets of the indices (s, k, p) give orthonormal bases B, and for these subsets there is an inversion formula:

$$f = \sum_{(s,k,p) \in B} \langle \psi_{skp}, f \rangle \psi_{skp}. \tag{2.1.1}$$

Wavelet packets are rarely constructed explicitly. More usually, one simply applies the fast discrete algorithm described in Reference [4] to the sampled values of f, and thereby produce the coefficients $w_{skp}(f)$. The underlying functions ψ can, however, be developed as follows. Introduce two (short) finite sequences $\{h_n\}$ and $\{g_n\}$, called *conjugate quadrature filters*, which satisfy the relations:

$$\sum_n h_{2n} = \sum_n h_{2n+1} = \frac{1}{\sqrt{2}}, \qquad g_n = -(-1)^n h_{1-n}, \qquad \text{for all } n; \tag{2.1.2}$$

$$\sum_n h_n h_{n+2m} = \sum_n g_n g_{n+2m} = \begin{cases} 1, & \text{if } m = 0, \\ 0, & \text{otherwise;} \end{cases} \tag{2.1.3}$$

$$\sum_n h_n g_{n+2m} = 0, \qquad \text{for all } m \in \mathbf{Z}. \tag{2.1.4}$$

Next, define a family of functions recursively for integers $k \geq 0$ by:

$$W_{2k}(x) = \sqrt{2} \sum_n h_n W_k(2x - n); \quad W_{2k+1}(x) = \sqrt{2} \sum_n g_n W_k(2x - n) \tag{2.1.5}$$

Note that W_0 satisfies a fixed-point equation. Conditions 2.1.2 through 2.1.4 ensure that a unique solution to this fixed-point problem exists, and that $\{W_k : k \in \mathbf{Z}\}$ forms an orthonormal basis for $L^2(\mathbf{R})$. The quadrature filter pair h, g can be chosen (see Reference [6]) so that the solution has any prescribed degree of smoothness.

Equations 2.1.2 through 2.1.5 all have periodic analogs as well, which can be used in the case of periodic boundary conditions. The experiments in this article used periodic algorithm with the so-called "C 6" coefficients, given as h_n and g_n in Table 1.

One-dimensional wavelet packets are defined from these W_k by the formula:

$$\psi_{skp}(x) = 2^{-s/2} W_k(2^{-s}x - p).$$

As described in Reference [4], taking those functions $\{\psi_{skp} : (s, k, p) \in \mathcal{I}\}$ for which the half-open *dyadic intervals* $\{[\frac{k}{2^s}, \frac{k+1}{2^s}) : (s, k, p) \in \mathcal{I}\}$ form a disjoint cover of the unit interval gives an orthonormal basis subset $\mathcal{I}$.

The library of basis functions in two dimensions consists of all possible tensor products of the ψ functions with both factors sharing the same scale s. The definitions and formulas for this two-dimensional case may be found in Reference [20]. Certain basis subsets can be described by disjoint tilings of the unit square, as follows. Let I be a half-open *dyadic square* $[\frac{k_x}{2^s}, \frac{k_x+1}{2^s}) \times [\frac{k_y}{2^s}, \frac{k_y+1}{2^s})$ and put $\psi_{I,(p_x,p_y)}(x, y) =$

Table 1. "Coiflet 6" coefficients for orthogonal wavelet packets.

n	Low-pass filter coefficient h_n	High-pass filter coefficient g_n
< 0	0	0
0	$3.85807777478867490 \times 10^{-2}$	$-2.26584265197068560 \times 10^{-1}$
1	$-1.26969125396205200 \times 10^{-2}$	$7.45687558934434280 \times 10^{-1}$
2	$-7.71615554957734980 \times 10^{-2}$	$-6.07491641385684120 \times 10^{-1}$
3	$6.07491641385684120 \times 10^{-1}$	$-7.71615554957734980 \times 10^{-2}$
4	$7.45687558934434280 \times 10^{-1}$	$1.26969125396205200 \times 10^{-2}$
5	$2.26584265197068560 \times 10^{-1}$	$-3.85807777478867490 \times 10^{-2}$
> 5	0	0

$2^{-s} s W_{k_x}(2^{-s}x - p_x) W_{k_y}(2^{-s}y - p_y)$. Then every basis in the library, for functions on the $2^S \times 2^S$ grid, corresponds to a set of the form:

$$\{\psi_{I,(p_x,p_y)} : I \in \mathcal{I}, p_x \in \mathbf{Z}, p_y \in \mathbf{Z}, 0 \le p_x < 2^{S-s}, 0 \le p_y < 2^{S-s}\},$$

where $\mathcal{I}$ is a disjoint cover of the unit square by such dyadic squares I, for $0 \le s \le S$ and $0 \le k_x, k_y < 2^{s-1}$.

A *graph basis* is a collection of wavelet packets corresponding to some disjoint cover $\mathcal{I}$ with squares no smaller than a fixed minimum. Computation of inner products with all such functions is performed recursively, with recursion depth controlled by the minimum square size. The *best basis* for a function f, chosen from among graph bases, is the one minimizing the entropy functional $H(a)$ of the expansion coefficients of f. The implementation of graph basis expansions and the best basis search algorithm is described in detail in Reference [19], sections 7.2 and 8.2. The entire procedure has complexity $O(N \log N)$ where N is the rank of the problem, and $N = 2^{2S}$ for the original grid-point formulation.

The function f can be approximated by f^ϵ, a superposition of just the largest components of its best-basis expansion. Call the best basis $\mathcal{I}_*$. The projection onto the top few coefficients is defined as follows:

$$f^\epsilon = \sum_{|a_I| > \epsilon} a_I \psi_I.$$

Here $I \in \mathcal{I}_*$, $a_I = \langle f, \psi_I \rangle$ and ϵ is some predetermined threshold. The summation over all integer translates (p_x, p_y) is suppressed for compactness.

The approximate value to be used for the theoretical dimension $TD(f)$ will be $TD(a) = \exp H(a)$. It makes little difference whether the full sequence for f or the truncated sequence for f^ϵ is used; truncation is mainly useful when analyzing infinite sequences.

2.2 Burgers' evolution equation with viscosity on the circle

Burgers' equation is the first part of the following initial value problem:

$$\frac{\partial F}{\partial t}(x,t) = -\frac{1}{2}\frac{\partial}{\partial x}F^2(x,t) + \nu \Delta F(x,t); \tag{2.2.1}$$

$$\left.\begin{aligned} F(x,0) &= F_0(x) \quad \text{for all } x; \\ F(x+1,t) &= F(x,t) \quad \text{for all } t \ge 0. \end{aligned}\right\} \tag{2.2.2}$$

The constant ν is the viscosity of the fluid and the function $F_0 = F_0(x)$ is the initial state at time $t = 0$.

Consider one classical example: $F_0(x) = \sin(2\pi x)$. The graph in Figure 1 shows the evolution from this initial function at times 0, 0.08, 0.16, 0.32, 0.5, 0.75, and 1.00. The two arcs of the sine, one positive the other negative, are propagating in opposite directions to produce a steep slope at $x = 32/64$.

The dissipation term ΔF produces the vanishing effect: the total energy in the solution tends to 0 as time increases. Without dissipation the slope at $x = 32/64$ would become infinite and a discontinuity would appear; the viscosity term controls how close the solution gets to singularity before dissipating. The apparition of a near-discontinuity means that the amplitudes of small-scale components in the solution are

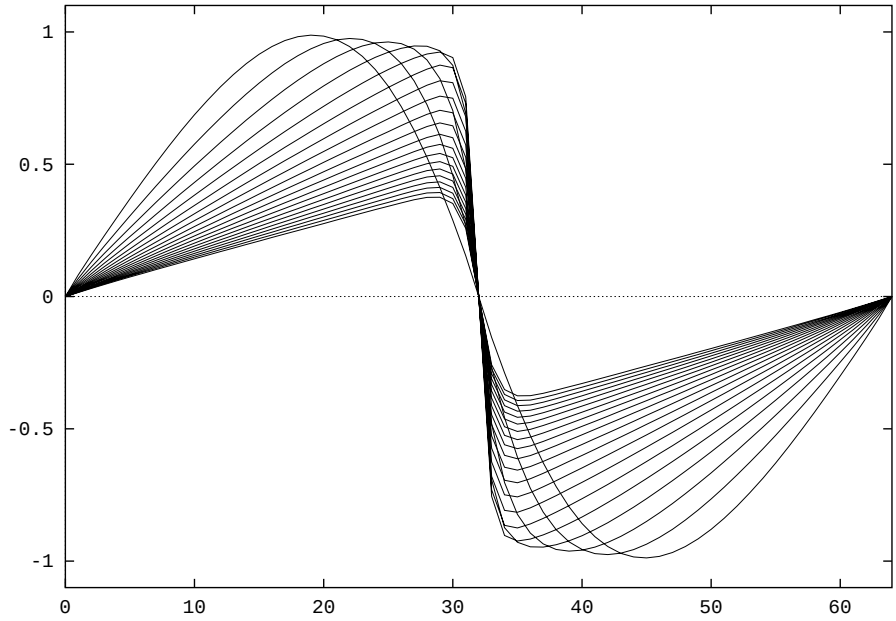

Figure 1. Burgers' evolution from $\sin(2\pi x)$ at $t = 0$ to $t = 1$ in increments of 0.05.

increasing, since they contribute the large derivatives. This phenomenon is better seen in Figure 2 below, which depicts the amplitudes of wavelet components of the signal arranged by scale.

The evolution was computed with a Godunov scheme applied to the 1-periodic signal, using a space-step of 1/64 and a time step of 1/100. In Reference [8], it was shown that the energy is decreasing in the biggest-scale wavelet components of the evolving function, while the energy in the smallest-scale ones is increasing. It was observed that one of the big-scale amplitudes already begins to decrease at time zero. The maxima of the smaller-scale amplitudes are reached later and later with decreasing scale. This last aspect can be better seen on Figure 2 which shows the absolute value of the wavelet coefficients in gray scale: white is zero, black is the maximum. The graduations between 0 and 100 represent time; the others show the index of the wavelet coefficients. The first wavelet coefficient is the mean of the signal (actually 0), the second is the biggest-scale difference coefficient, the third and fourth are next-largest difference coefficients, and so on. The last 32 are the smallest scale difference coefficients, since there are a total of 64 samples of the signal. The analysis was done with "Coiflet 30" wavelets [6] because they have a large number of vanishing moments and are nearly symmetric.

Ultimately, through dissipation, the function and thus all its wavelet coefficients decrease to 0.

2.3 Two-dimensional incompressible Navier–Stokes simulations on the torus

The classical simulation of two-dimensional decaying turbulent flows uses the incompressible Navier–Stokes equation with small viscosity. The Kraichnan–Batchelor theory in this situation [1, 9] postulates homogeneous mixing within the flow and supposes that the whole vorticity field is involved in the "cascade process" that transports enstrophy from large eddies to small ones, while energy is transferred from small to large scales.

In contrast to this explanation, we believe that two-dimensional turbulent flows are generically inhomogeneous and propose to model them as a superposition of coherent rotational vortices embedded in a random quasi-irrotational flow. We have observed, in numerical simulations of two-dimensional Navier–Stokes equations with random initial conditions, that isolated vortices result from the condensation of enstrophy into localized, well-separated structures. These structures are stable as long as they do not interact with one

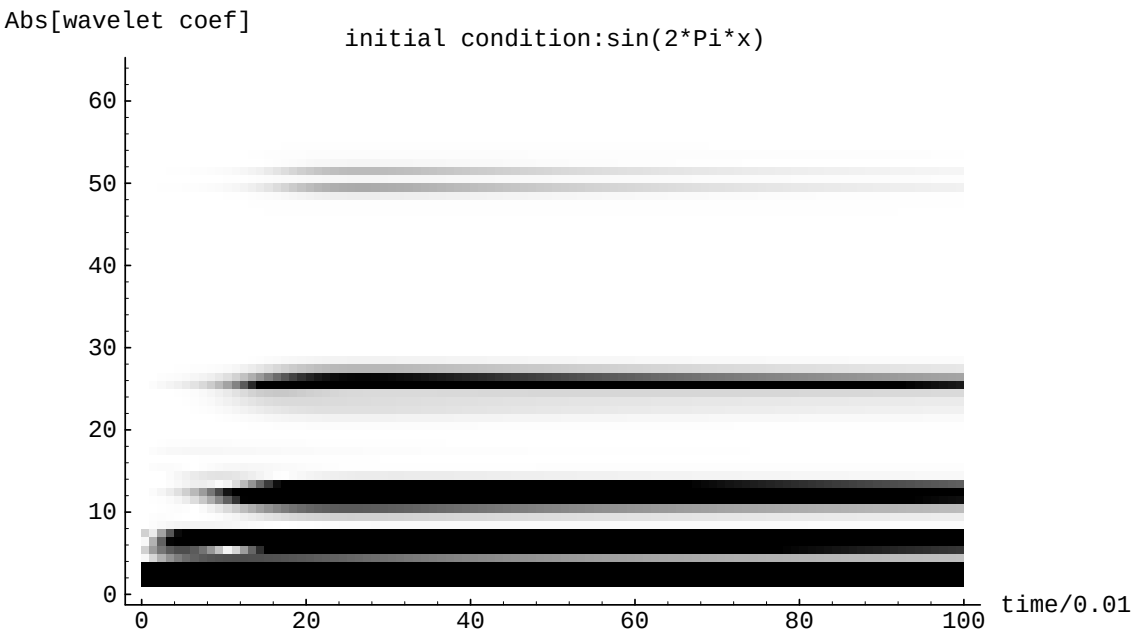

Figure 2. Amplitudes of the wavelet coefficients of Burgers' evolution from the initial function $\sin(2\pi x)$, shown in gray scale.

another, but during close encounters they experience strong deformations, which then excite some internal degrees of freedom. This gives rise to a local *cascade* or transfer of enstrophy toward small scales and to its concomitant dissipation. Consequently, only a limited *active portion* of the vorticity field, correlated to the coherent vortices, is responsible for the turbulent cascade. The remainder, or *background portion* of the field, is passively advected and plays a negligible dynamical role.

The *atomic* view may be compared with the vortex methods of Winckelmans and Leonard [22], Marchioro and Pulvirenti [14], and Saffman [17]. It generalizes the simplest model used to approximate two-dimensional flows, that of superposed *point vortices*, by considering the flow to be a superposition of *atoms* that are chosen from among a library of smooth localized functions such as wavelet packets [4] or localized cosine functions [3, 13]. The additional parameters available to these atoms enable us to take into account the internal degrees of freedom of each vortex, which can be considered as a *molecule*.

The goal will be to compute the number of "significant" atoms in a turbulent flow, *i.e.*, those components whose amplitudes exceed a preset threshold. Those that correspond to the same locale can be interpreted as the principal components of a coherent structure. Their number evolves in time, with a generally decreasing trend due to the decay in enstrophy caused by dissipation, and gives a quantitative estimate of the number of coherent structures and the complexity of the turbulent flow.

The analysis begins with a direct numerical solution of the Navier–Stokes equation describing the dynamics of a two-dimensional incompressible viscous flow. In the periodic plane $S = (0, 2\pi) \times (0, 2\pi) \subset \mathbf{R}^2$ and in the absence of external forcing, these take the following form:

$$\begin{aligned} \frac{\partial \mathbf{u}}{\partial t} + (\mathbf{u} \cdot \nabla)\mathbf{u} + \nabla P - \nu \nabla^2 \mathbf{u} = 0, &\qquad \text{in } S \times \mathbf{R}^+, \\ \nabla \cdot \mathbf{u} = 0, &\qquad \text{in } S \times \mathbf{R}^+, \\ \mathbf{u}(\mathbf{x}, 0) = \mathbf{u}_0(\mathbf{x}), &\qquad \text{in } S. \end{aligned}$$

Here $\mathbf{u}$ is the velocity field, P is the pressure field, and ν is the kinematic viscosity. Periodic boundary conditions are also imposed. The equations are rewritten in terms of *vorticity* ω and *stream function* ψ,

defined by

$$\mathbf{u} = \begin{pmatrix} u_1 \\ u_2 \end{pmatrix} = \begin{pmatrix} -\frac{\partial \psi}{\partial x_2} \\ \frac{\partial \psi}{\partial x_1} \end{pmatrix}; \qquad \omega = \frac{\partial \mathbf{u}_2}{\partial x_1} - \frac{\partial \mathbf{u}_1}{\partial x_2}. \tag{2.3.1}$$

The Navier–Stokes equations then become

$$\begin{aligned} \frac{\partial \omega}{\partial t} + J(\psi, \omega) - \nu \nabla^2 \omega = 0, \qquad & (\mathbf{x}, t) \in S \times \mathbf{R}^+; \\ \omega = \nabla^2 \psi, \qquad & (\mathbf{x}, t) \in S \times \mathbf{R}^+; \\ \omega(\mathbf{x}, 0) = \omega_0(\mathbf{x}), \qquad & \mathbf{x} \in S. \end{aligned}$$

Again, periodic boundary conditions are imposed. The Jacobian operator in terms of these new variables is:

$$J(\psi, \omega) = \frac{\partial \psi}{\partial x_1} \frac{\partial \omega}{\partial x_2} - \frac{\partial \psi}{\partial x_2} \frac{\partial \omega}{\partial x_1}. \tag{2.3.2}$$

The functions ω and ψ can be expanded in their Fourier series over the periodic domain S:

$$\begin{aligned} \omega(\mathbf{x}, t) &= \sum_{\mathbf{k}} \hat{\omega}(\mathbf{k}, t) e^{i \mathbf{k} \cdot \mathbf{x}}, \qquad \hat{\omega}(\mathbf{k}, t) = \frac{1}{2\pi} \int_{\mathbf{x} \in S} \omega(\mathbf{x}, t) e^{-i \mathbf{k} \cdot \mathbf{x}} \, d\mathbf{x}; \\ \psi(\mathbf{x}, t) &= \sum_{\mathbf{k}} \hat{\psi}(\mathbf{k}, t) e^{i \mathbf{k} \cdot \mathbf{x}}, \qquad \hat{\psi}(\mathbf{k}, t) = \frac{1}{2\pi} \int_{\mathbf{x} \in S} \psi(\mathbf{x}, t) e^{-i \mathbf{k} \cdot \mathbf{x}} \, d\mathbf{x}. \end{aligned}$$

A turbulent vorticity field such as the one depicted in Figure 3 develops from a random initial vorticity field $\omega_0(\mathbf{x})$ which is integrated for many time steps in the presence of time-periodic external forcing (at very low wavenumbers), until the vorticity field reaches a statistically steady state. Forcing is subsequently turned off and the same integration is continued in the decaying regime.

A pseudo-spectral Galerkin method was used to integrate the Navier–Stokes equations; at each time step, all differentiation was performed in $\hat{\omega}, \hat{\psi}$ coordinates and all multiplication in ω, ψ coordinates. Both ω and ψ are represented as finite Fourier series, or superpositions of the Fourier modes at wavenumbers $0 \leq |\mathbf{k}| < k_r$, where k_r is the cutoff wavenumber which gives some fixed resolution. The time integration was done using an Adams–Bashforth scheme. The periodic plane S was sampled on 128^2 grid points in the simulation. This is not terribly fine, so the commonly-used mechanism of *modeling subgrid dissipation* was employed to incease the apparent resolution.

The subgrid scale model was a hyperdissipation operator $-(-\nabla^2)^4$, which replaced the Laplacian operator in the Navier–Stokes equations. This caused the vorticity field produced by the direct numerical simulation to decay more rapidly in regions of high local variation than it would in a simulation using Laplacian dissipation. The disproportionately fast decay produced a flow that acts "as if" energy losses from subgrid scales were included in each time step through aliasing.

The program ran for 6000 time steps $\Delta t = 10^{-4}$ in units of T^1, which corresponds to about 30 initial eddy-turnover times, starting from the statistically steady state. The vorticity fields analyzed here are time slices spaced 20 time steps apart. These may be considered to be typical snapshots of a fully-developed turbulent flow whose enstrophy is slowly decaying.

§3 Results

3.1 One-dimensional results: Burgers' equation

The periodic solution to the 1-periodic Burgers' equation from an initial state $F_0(x) = \sin(2\pi x)$ was computed using a viscosity of $\nu = 0.01/\pi$, from $t = 0$ to $t = 1$. The results are plotted at time intervals of 0.05 in Figure 1, and the amplitudes of the associated wavelet coefficients are depicted as gray levels in Figure 2. The number of dark streaks in the latter figure give a crude estimate for the theoretical dimension of the solution.

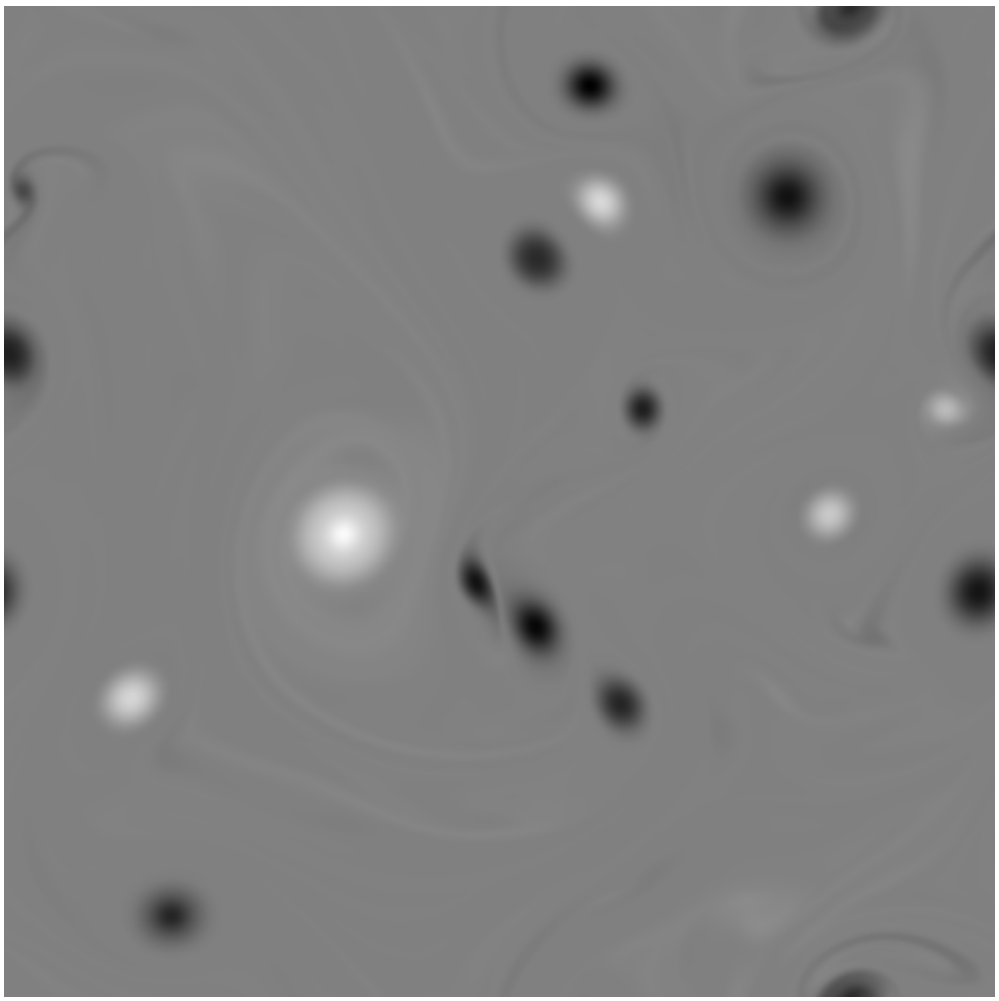

Figure 3. Vorticity field at an instant of time, scaled to fill an 8-bit dynamic range.

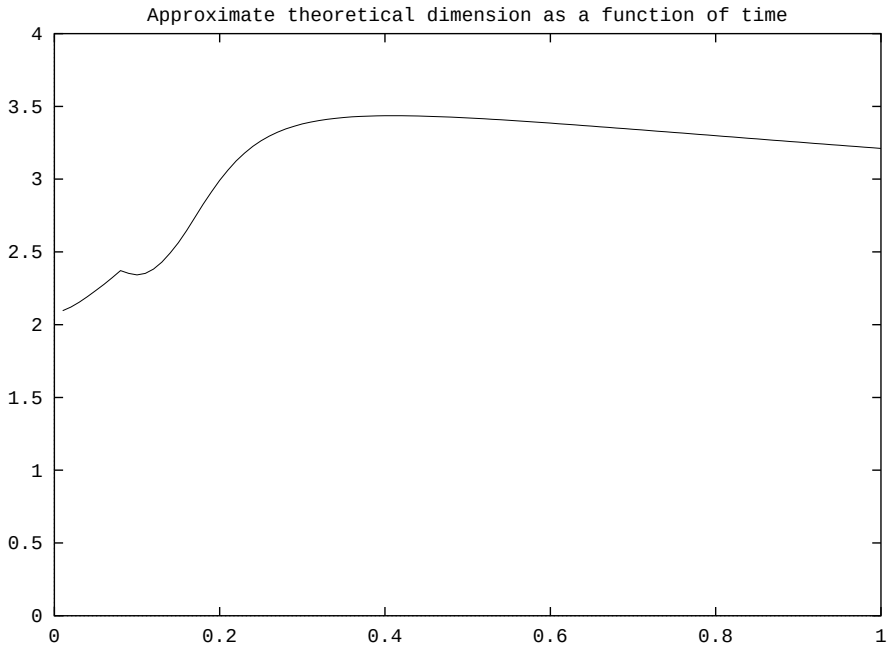

Figure 4. Theoretical dimension of a solution of Burgers' equation from an initial state $\sin(2\pi x)$ at $t = 0$ to $t = 1$.

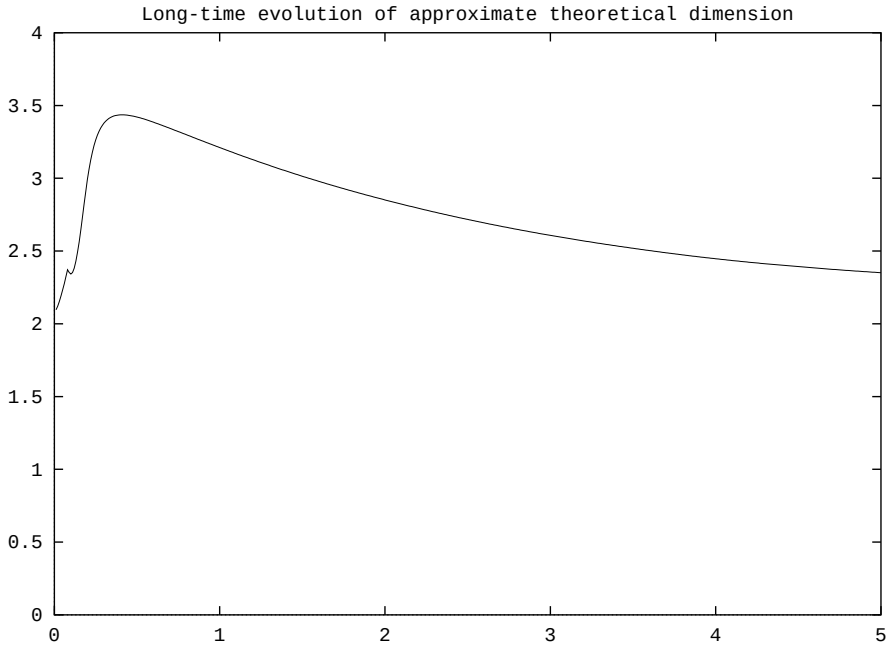

Figure 5. Theoretical dimension of a solution of Burgers' equation from an initial state $\sin(2\pi x)$ at $t = 0$ to $t = 5$.

The theoretical dimension was approximated somewhat better with the best-basis expansion using Coiflet 6 wavelet packets as phase atoms. This was done at every time step, with $\Delta t = 0.01$. The result is plotted in Figure 4. A longer-term plot of theoretical dimension is seen in Figure 5.

It is readily noticed that the estimated theoretical dimension jumps from about 2 to about 3.5 at first, as the shock begins to form at spatial position 32, then decreases back to 2 as dissipation smooths out the function and removes the large derivatives. Extra phase atoms of small position variance and large frequency variance seem to be needed to represent large derivatives near the shock, whereas the phase atoms which represent the two smooth lobes of the initial sine curve remain as a kind of background, persisting even to long times when the solution has dissipated nearly to 0.

The peculiar feature at time $t = 0.08$ may be the result of a sudden change of the basis in which the atomic decomposition is performed. The best orthogonal basis changes at that instant from a 21-subband decomposition to a 10-subband decomposition.

Even crude approximations of theoretical dimension provide some clue to the number of degrees of freedom required to approximate a solution to a complicated evolution equation. In the one-dimensional Burgers' equation with dissipation, even the wavelet decomposition provides a reasonable estimate of the number of phase atoms in the minimal decomposition. As the shock begins to form, extra wavelet components appear at the small scales indexed by ordinate values near 50 in Figure 2. These decay as the energy dissipates and the sharp slope near abscissa 32 in Figure 1 becomes smoother.

3.2 Two-dimensional results: Navier–Stokes equation

Now consider a vorticity field, similar to that depicted in Figure 3, representing what we believe is a generic time slice of a homogenous, isotropic, fully developed two-dimensional turbulent flow. The experiment segmented it into high-enstrophy and low-enstrophy components in the wavelet packet best basis.

All experiments began with an initial condition consisting of a fully-developed two-dimensional turbulent flow sampled on 128^2 grid points. This gave a "reference initial flow field" which was then evolved for an additional 6000 time steps between $t = 0.0$ and $t = 0.6$, using the Navier–Stokes model described in the previous section. In the chosen normalization, this interval is approximately 30 eddy turnover times, or the time it takes for an average vortex to make 30 rotations. The resulting evolution may be called the "reference flow field evolution". Vorticity fields were computed at 300 equally-spaced future times and then their theoretical dimension was estimated in the wavelet packet best basis defined by the "Coiflet 6" filters listed in Table 1. In Figure 6 may be seen the evolution of theoretical dimension for this reference evolution.

There are fluctuations in the estimated theoretical dimension which cause the graph to depart from its course of smooth decay. These are caused both by sudden changes in the basis choice and by the lack of shift-invariance of the orthogonal wavelet packet expansion.

The theoretical dimension estimate starts at approximately 400 for a field with 26 distinguishable vortices and decays to 150 at the 301st time slice when there are 15. The count of vortices is necessarily subjective, and no attempt was made to include the contribution of *vortex filaments* which also evolve and decay in the simulation.

The evolution of theoretical dimension measures the quality of an approximate evolution from a projected initial state [7]. Figure 7 shows the evolution of estimated theoretical dimension from initial states approximated by 50%, 5%, and 0.5% of the original components. These represent 8192, 819, and 82 degrees of freedom, respectively. Table 2 shows how initial and final estimates of theoretical dimension compare with the subjective count of significant vortices in the original and the three approximations.

By contrast, the portion of the initial vorticity field which was discarded by the projection onto strong wavelet packet components contains a very large number of local vorticity extrema. The theoretical dimension estimate for those weak *remainder* fields are plotted in Figure 8, which shows the 50%, 95%, and 99.5% leftovers from Figure 7. Notice that the remainder theoretical dimensions are much larger than those for the approximations. Table 3 compares the estimate of those theoretical dimensions with a crude subjective count of significant vortices.

Small fluctuations of the theoretical dimension estimate are due to the lack of shift-invariance of wavelet and wavelet packet decompositions. This problem can be alleviated by computing $TD(f)$ as the minimum of the information costs of the best basis wavelet packet expansions of $f(x - x_0)$, where x_0 ranges over several small spatial shifts. That algorithm seems to have $O(N^2)$ complexity, though there is a well-known

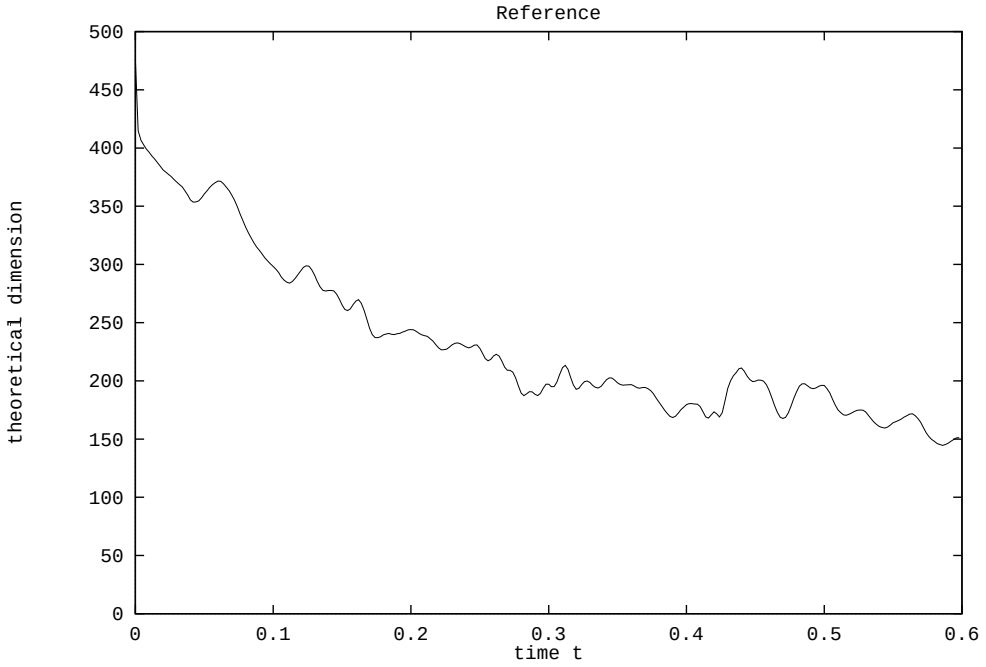

Figure 6. Evolution of estimated theoretical dimension for the original vorticity field.

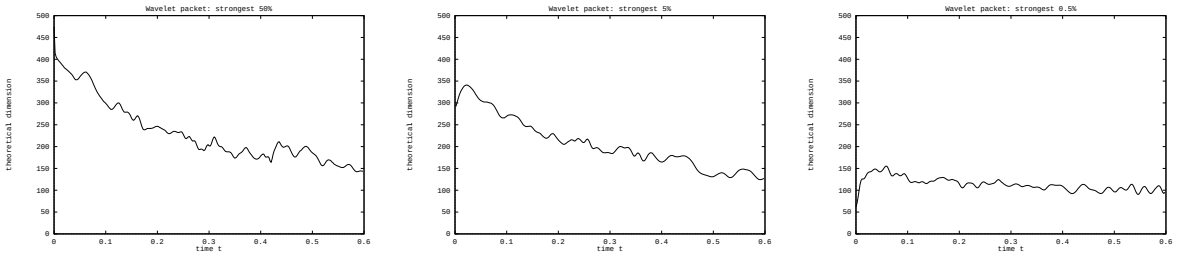

Figure 7. Evolution of estimated theoretical dimension for the vorticity field reconstructed from: (left) the top 50%, or 8192; (middle) the top 5%, or 819; (right) the top 0.5%, or 82 of the original's wavelet packet components.

Table 2. Subjective count of vortices (VC_t) compared with theoretical dimension (TD_t) at time t for 2-D decaying evolutions from increasingly simplified initial turbulent vorticity fields. Times $t = 0.020$ and $t = 0.598$ were chosen slightly inside the simulation interval $[0.0, 0.6]$ to avoid artifacts.

Components	Fraction	$VC_{.020}$	$TD_{.020}$	$VC_{.598}$	$TD_{.598}$
16384	100%	26	381	15	151
8192	50%	26	381	15	143
819	5%	21	340	17	127
82	0.5%	20	135	19	95

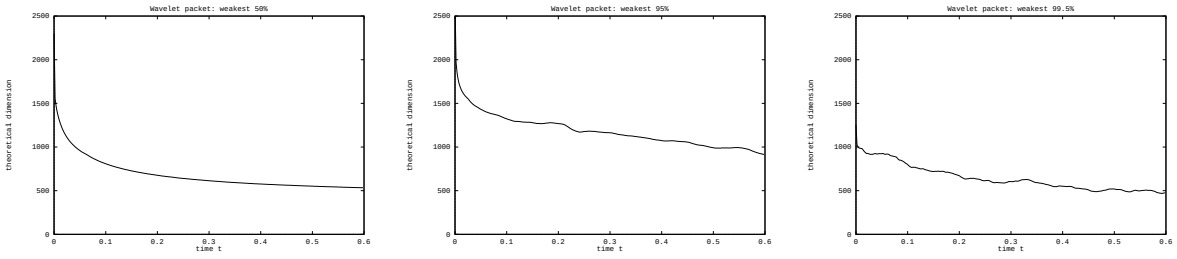

Figure 8. Evolution of estimated theoretical dimension for the vorticity field reconstructed from: (left) the bottom 50%, or 8192; (middle) the bottom 95%, or 15564; (right) the bottom 99.5%, or 16302 of the original's wavelet packet components.

Table 3. Subjective count of vortices (VC) compared with theoretical dimension (TD) for 2-D decaying evolutions from the increasingly energetic remainders of simplified initial turbulent vorticity fields.

Components	Fraction	$VC_{.020}$	$TD_{.020}$	$VC_{.598}$	$TD_{.598}$
16384	100%	26	381	15	151
8192	50%	600	1160	100	534
15564	95%	350	1583	150	915
16302	99.5%	200	927	60	477

shift-invariant wavelet expansion [2, 19] with complexity $O(N \log N)$ which may be used when wavelet phase atoms suffice.

§4 Discussion

This paper describes very crude approximations to the theoretical dimension of a complicated evolution, yet even these provide some clue to the complexity of the flow. Still, many improvements of the computation are possible.

The most basic improvement would be to compute theoretical dimension with a larger library of phase atoms. For example, Gabor functions could be used as in the matching pursuit algorithm. However, this would raise the complexity of estimating TD on an N-point grid to $O(N^2)$. A faster improvement would be to use best-basis with multiple wavelet packet libraries, possibly combined with adapted local cosine libraries or other modern basis sets. This would result in an algorithm of complexity $O(N[\log N]^2)$, with a constant that grew with the number of distinct libraries searched. Moving still closer to matching pursuit, the requirement of using a best orthogonal basis could be relaxed and a best atomic decomposition could be sought instead, using the adapted waveform meta-algorithm.

Since wavelet and more generally wavelet packet algorithms are not shift-invariant, their estimates of TD will always contain small fluctuations depending upon details of grid spacing and the motions of coherent parts of the analyzed function. There are several ways to avoid this, all of which increase the complexity of the computation by finding the minimal estimate of TD over a family of shifts. When wavelet phase atoms are used, the added complexity is minimal.

Phase atom decompositions provide a tool for locating and measuring coherent parts of a flow. A coherent structure is said to be present at a point when a small number of large phase atoms are supported near that point; the number of these atoms gives an estimate for the number of degrees of freedom in the coherent structure. This definition, together with techniques from wavelet packet analysis, provides an algorithm to extract portions of flows that human observers see as "coherent."

Theoretical dimension is useful in deciding both how many degrees of freedom are actually present in the coherent part of a function, and to determine the minimal rank of a projection onto a good approximate solution. Furthermore, the theoretical dimension of components discarded by such a projection are an indicator of the quality of the approximation. When the theoretical dimension of the discarded components is too low, it means that the discarded portion contains some coherent part.

Since the computation of theoretical dimension is relatively cheap, it may be done alongside simulations and computed evolutions simply as a guide to some global properties of complicated phenomena.

Acknowledgments. The work of the second and third authors was supported in part by the NATO program *Collaborative Research*, contract CRG-930456. The first author was supported in part by AFOSR contract F49620-92-J-0106, NSF grant DMS-9302828, and a private grant from the Southwestern Bell Telephone Company. The Burgers' equation simulation was prepared with *Mathematica* on a NeXT computer at Washington University by Frédéric Heurtaux and Fabrice Planchon, who were supported in part by the Internship Office of the École Polytechnique. The Navier–Stokes equation simulations were performed on the Cray 2 at the Centre de Calcul Vectoriel pour la Recherche, using the incompressible Navier-Stokes code of Claude Basdevant. Theoretical dimension and best-basis wavelet packet expansions in one and two dimensions were performed using two versions of the Adapted Wavelet Analysis Library [18, 21].

References

[1] George K. Batchelor. Computation of the energy spectrum in homogeneous two-dimensional turbulence. *Physics of Fluids*, 12(Supplement II):233–239, 1969.

[2] Gregory Beylkin. On the representation of operators in bases of compactly supported wavelets. *SIAM Journal of Numerical Analysis*, 6-6:1716–1740, 1992.

[3] Ronald R. Coifman and Yves Meyer. Remarques sur l'analyse de Fourier à fenêtre. *Comptes Rendus de l'Académie des Sciences de Paris*, 312:259–261, 1991.

[4] Ronald R. Coifman, Yves Meyer, Stephen R. Quake, and Mladen Victor Wickerhauser. Signal processing and compression with wavelet packets. In Yves Meyer and Sylvie Roques, editors, *Progress in Wavelet Analysis and Applications*, Proceedings of the International Conference "Wavelets and Applications," Toulouse, France, 8–13 June 1992, pages 77–93. Editions Frontieres, Gif-sur-Yvette, France, 1993.

[5] Ronald R. Coifman and Mladen Victor Wickerhauser. Entropy based algorithms for best basis selection. *IEEE Transactions on Information Theory*, 32:712–718, March 1992.

[6] Ingrid Daubechies. Orthonormal bases of compactly supported wavelets. *Communications on Pure and Applied Mathematics*, XLI:909–996, 1988.

[7] Marie Farge, Eric Goirand, Yves Meyer, Frédéric Pascal, and Mladen Victor Wickerhauser. Improved predictability of two-dimensional turbulent flows using wavelet packet compression. *Fluid Dynamics Research*, 10:229–250, 1992.

[8] Frédéric Heurtaux, Fabrice Planchon, and Mladen Victor Wickerhauser. Scale decomposition in Burgers' equation. In John J. Benedetto and Michael Frazier, editors, *Wavelets: Mathematics and Applications*, Studies in Advanced Mathematics, pages 505–523. CRC Press, Boca Raton, Florida, 1992.

[9] Robert H. Kraichnan. Inertial ranges in two-dimensional turbulence. *Physics of Fluids*, 10:1417–1423, 1967.

[10] Fazal Majid. Applications des paquets d'ondelettes au débruitage du signal. Preprint, Department of Mathematics, Yale University, 28 July 1992. Rapport d'Option, Ecole Polytechnique.

[11] Stéphane G. Mallat. A theory for multiresolution signal decomposition: The wavelet decomposition. *IEEE Transactions on Pattern Analysis and Machine Intelligence*, 11:674–693, 1989.

[12] Stéphane G. Mallat and Zhifeng Zhang. Matching pursuits with time-frequency dictionaries. *IEEE Transactions on Signal Processing*, 41(12):3397–3415, December 1993.

[13] Henrique Malvar. Lapped transforms for efficient transform/subband coding. *IEEE Transactions on Acoustics, Speech, and Signal Processing*, 38:969–978, 1990.

[14] C. Marchioro and M. Pulvirenti. *Vortex Methods in 2D Fluid Dynamics*. Number 203 in Lecture Notes in Physics. Springer-Verlag, Berlin, 1984.

[15] Yves Meyer. Orthonormal wavelets. In Jean-Michel Combes, Alexander Grossmann, and Philippe Tchamitchian, editors, *Wavelets: Time-Frequency Methods and Phase Space*, pages 21–37. Springer-Verlag, Berlin, second edition, 1989.

[16] Yves Meyer. *Wavelets: Algorithms and Applications*. SIAM Press, Philadelphia, 1993.

[17] Philip Saffman. Vortex interactions and coherent structures in turbulence. In R. E. Meyer, editor, *Transition and Turbulence*. Academic Press, 1981.

[18] Mladen Victor Wickerhauser. *Adapted Waveform Analysis Library, v2.0*. Fast Mathematical Algorithms and Hardware Corporation, Hamden, Connecticut, June 1992. Software Documentation.

[19] Mladen Victor Wickerhauser. *Adapted Wavelet Analysis from Theory to Software*. AK Peters, Ltd., Wellesley, Massachusetts, 9 May 1994. With optional diskette.

[20] Mladen Victor Wickerhauser. Comparison of picture compression methods: Wavelet, wavelet packet, and local cosine transform coding. In Charles K. Chui, Laura Montefusco, and Luigia Puccio, editors, *Wavelets: Theory, Algorithms, and Applications*, Proceedings of the International Conference in Taormina, Sicily, 14–20 October 1993, pages 585–621. Academic Press, San Diego, California, 1994.

[21] Mladen Victor Wickerhauser. *AWA 3: Adapted Wavelet Analysis Library, version 3*. Fast Mathematical Algorithms and Hardware Corporation, Hamden, Connecticut, June 1995. Software Documentation.

[22] G. S. Winckelmans and A. Leonard. Contributions to vortex particle methods for the computation of three-dimensional incompressible unsteady flows. *Journal of Computational Physics*, 109:247–273, 1993.